

Cite this: *Nanoscale*, 2018, **10**, 21617

## Recent progress in transition metal phosphides with enhanced electrocatalysis for hydrogen evolution

Huitong Du,<sup>a</sup> Rong-Mei Kong,<sup>a</sup> <sup>a</sup> Xiaoxi Guo,<sup>a</sup> Fengli Qu <sup>\*a</sup> and Jinghong Li <sup>b</sup>

Increasing demand for hydrogen energy has boosted the exploration of inexpensive and effective catalysts. Transition metal phosphides (TMPs) have been proven as excellent catalysts for the hydrogen evolution reaction (HER). Very recently, the search for TMP-based catalysts has been mainly directed at enhanced electrocatalytic performance. Hence, a concluded guideline for enhancing HER activity is highly desired. In this mini review, we briefly summarize the most recent and instructive developments in the design of TMP-based catalysts with enhanced electrocatalysis for hydrogen evolution from composition and structure engineering strategies. These strategies and perspectives are also meaningful for designing other inexpensive and high-performance catalysts.

Received 28th September 2018,

Accepted 28th October 2018

DOI: 10.1039/c8nr07891b

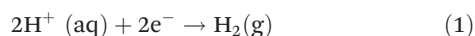
rsc.li/nanoscale

### 1. Introduction

The increasing global energy crisis and accompanying environmental issues are motivating scientists to search for eco-friendly and sustainable energy sources to substitute conventional fossil fuels.<sup>1,2</sup> Hydrogen, as an abundant and clean energy source, is advocated as a promising future energy source candidate.<sup>3</sup> At present, the steam reforming of fossil fuels still remains the dominant route to the large-scale production of hydrogen. Nevertheless, this process aggravates the consumption of fossil fuels and thus results in a large amount of CO<sub>2</sub> emission.<sup>4,5</sup> Thence, the economical and renewable route to producing hydrogen appeals more research interest.<sup>6</sup> One potential sustainable way to accomplish this is electrochemical water splitting.<sup>7-10</sup>

The hydrogen evolution reaction (HER) is the cathodic half-cell reaction of water splitting. It has been extensively studied by virtue of its advantages such as using water as the reactant, considerable hydrogen generation efficiency and no emission of greenhouse gases.<sup>11-13</sup> As described by eqn (1) and (2), this reaction realizes the production of hydrogen gas through the reduction of protons and water molecules.

In acidic media:



In alkaline media:



Generally, the HER process proceeds by a multistep pathway with two possible mechanisms in acidic media.<sup>14-16</sup> The guiding mechanism in the HER can be theoretically revealed by the Tafel slope value. In the first step, an electron is transferred to the catalyst surface to form an intermediate adsorbed hydrogen atom. This process is called the discharge reaction or Volmer reaction:

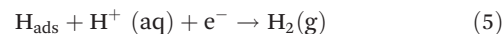


The Tafel slope for this reaction can be indicated as:

$$b_{1,\text{V}} = 2.303RT/\alpha F \quad (4)$$

where  $R$  is the ideal gas constant,  $T$  is the absolute temperature,  $\alpha$  is the symmetry coefficient with a value of 0.5 and  $F$  is the Faraday constant.

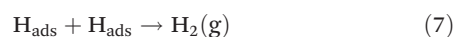
The subsequent step proceeds through two different routes to evolve the H<sub>2</sub> molecule. One possible route is that an adsorbed hydrogen atom combines with a second electron and another proton to form a H<sub>2</sub> molecule, which is known as the electrochemical desorption reaction or Heyrovsky reaction:



And its Tafel slope can be indicated as:

$$b_{2,\text{H}} = 2.303RT/(1 + \alpha)F \quad (6)$$

Another possibility is the recombination of two adsorbed hydrogen atoms on the catalyst surface *via* the Tafel reaction, also known as the chemical desorption step:



<sup>a</sup>College of Chemistry and Chemical Engineering, Qufu Normal University, Qufu 273165, Shandong, China. E-mail: fengliquhn@hotmail.com

<sup>b</sup>Department of Chemistry, Tsinghua University, Beijing 100084, China

And its Tafel slope can be indicated as:

$$b_{2,T} = 2.303RT/2F \quad (8)$$

The deduced Tafel slope values of the above reactions at 25 °C are 118 mV dec<sup>-1</sup>, 39 mV dec<sup>-1</sup> and 29 mV dec<sup>-1</sup> for  $b_{1,v}$ ,  $b_{2,H}$  and  $b_{2,T}$ , respectively. When a catalyst is used for the acidic HER with a measured Tafel slope value of 29 mV dec<sup>-1</sup>, this result suggests that the electrochemical desorption step is the rate-limiting step, and this catalytic process tends to follow the Volmer–Tafel mechanism.

In practice, the standard reduction potential of the HER is defined as  $E^\circ = 0$  V vs. normal hydrogen electrode at pH = 0.<sup>17,18</sup> However, electrochemical reactions need to overcome the kinetic energy barrier like many chemical reactions. Thus, the assistance of catalysts is essential to make the HER more energy-efficient. Overpotential is regarded as a key factor to evaluate the performance of catalysts.

Currently, platinum (Pt) is considered to be the best HER catalyst with a minimum overpotential, but the limited storage and expensive price hinder its widespread use. As stated above, it is highly desirable to develop non-noble metal catalysts. Transition metal phosphides (TMPs) emerge as typical representatives of highly active and inexpensive HER catalysts, and several TMPs have been proven as promising catalysts for HER, including CoP,<sup>11,19–23</sup> Ni<sub>2</sub>P,<sup>24–26</sup> MoP,<sup>27–29</sup> Cu<sub>3</sub>P,<sup>30</sup> FeP<sup>31,32</sup> and Ni<sub>5</sub>P<sub>4</sub>.<sup>33</sup> Liu *et al.* predicted that Ni<sub>2</sub>P was a decent HER catalyst by density functional theory (DFT) calculations in 2005.<sup>34</sup> The first experimental report on TMP catalysts for hydrogen evolution was published by the Zhang group in 2013.<sup>35</sup> FeP porous nanosheets were synthesized through the anion exchange reaction of inorganic–organic hybrid Fe<sub>18</sub>S<sub>25</sub>–TETAH nanosheets with P ions and showed impressive catalytic activity with a low overpotential and small Tafel slope value in 0.5 M H<sub>2</sub>SO<sub>4</sub> (Fig. 1A–C). Subsequently, the counts of published studies on TMPs for the HER continued increasing. Sun and coworkers reported that the different TMP nanoarrays grew on three-dimensional substrates with enhanced catalytic activity for the HER.<sup>11,30,31,36,37</sup> For example, the CoP nanowire array was fabricated and presented an outstanding HER performance at all pH values (Fig. 1D).<sup>11</sup> These groundbreaking studies open up the golden era of TMPs, making them promising and efficient HER catalysts. Very recently, the research interest for TMP-based catalysts has been mainly directed at enhanced electrocatalytic performance. There still exist many strategies to further improve their HER activity, however, there is currently no guideline for systematically improving their electrocatalytic activity.

In this mini review, we briefly summarize the most recent and instructive developments in the design of TMP-based catalysts with enhanced catalytic activity for the HER and present a selected summary of their HER performance (Table 1). These strategies and perspectives are also meaningful for designing other inexpensive and high-performance catalysts.

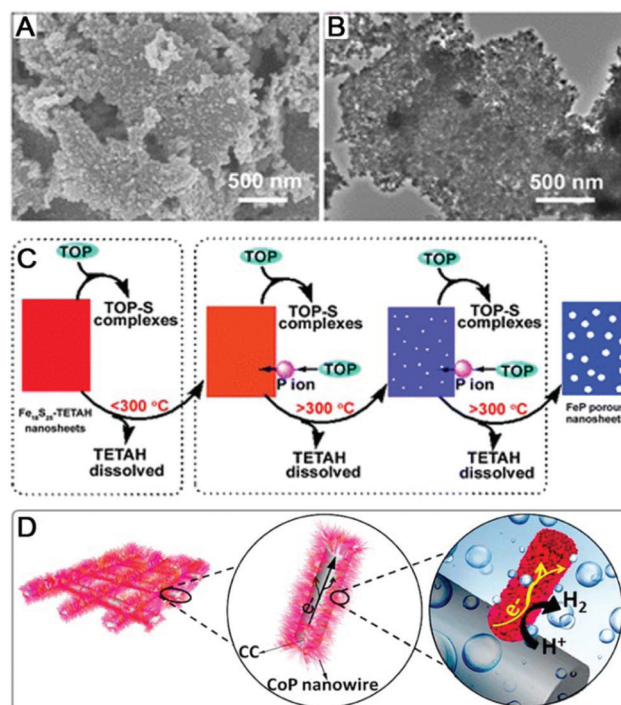


**Fig. 1** (A) Scanning electron microscopy (SEM) image and (B) transmission electron microscopy (TEM) image of the FeP nanosheets. (C) Scheme illustrating the synthesis of the porous FeP nanosheets through the anion exchange reaction of the inorganic–organic hybrid Fe<sub>18</sub>S<sub>25</sub>–TETAH nanosheets with P ions. Reproduced with permission from ref. 35, Copyright 2013 Royal Society of Chemistry. (D) Schematic illustration of CoP nanowires array for the HER. Reproduced with permission from ref. 11, Copyright 2014 The American Chemical Society.

## 2. Composition engineering for enhancing HER performance

Introducing elements into TMPs has been reported as an effective approach to improve the catalytic activity of catalysts by means of tuning the electronic structure and optimizing the adsorption energy of intermediates.<sup>38</sup> Composition engineering can be divided into metallic element doping, non-metallic element doping and hybridization with other compositions.

### 2.1. Metallic element doping

Doping TMPs with metallic elements (such as Zn, Co, Fe, Mn, Al and Mo) is a customary way to enhance their catalytic activity.<sup>39–44</sup> Wu *et al.* successfully doped Mo into CoP nanoarrays and explored its origin by density functional theory (DFT) calculations.<sup>40</sup> The Mo-doped CoP was synthesized by a metal organic frame (MOF)-derived route and the resulting catalyst demanded an overpotential of 40 mV to reach 10 mA cm<sup>-2</sup>, 120 mV less than that for CoP/CC (Fig. 2A–D). The DFT calculations indicated that the reason for the enhanced intrinsic catalytic activity might be the energy barrier lowered through Mo doping (Fig. 2E). The Chen group developed Mn-doped Ni<sub>2</sub>P nanosheets as an efficient catalyst for enhanced HER at

**Table 1** Selected summary of the HER performance of some recent TMP-based catalysts

Catalyst	Substrate	Electrolyte	Overpotential (mV)		Tafel slope (mV dec <sup>-1</sup> )	Ref.
			$\eta_{10}$	$\eta_{20}$		
Al-Ni <sub>2</sub> P	Ti mesh	1.0 M KOH	129		98	39
Mo-CoP	Carbon cloth	1.0 M KOH	40		65	40
Mn-Ni <sub>2</sub> P	Carbon cloth	1.0 M KOH	97		61	42
Zn <sub>0.04</sub> Co <sub>0.96</sub> P	Ti mesh	0.5 M H <sub>2</sub> SO <sub>4</sub>	39		46	43
N-CoP	Carbon cloth	0.5 M H <sub>2</sub> SO <sub>4</sub>	42		41.2	45
MoP S	Ti foil	0.5 M H <sub>2</sub> SO <sub>4</sub>	64	78	50	47
Ni <sub>2</sub> P-CoP	Carbon cloth	0.5 M H <sub>2</sub> SO <sub>4</sub>	85		40	49
FeP/Ni <sub>2</sub> P	Ni foam	1.0 M KOH	14		24.2	50
Cu <sub>3</sub> P-CoP	Carbon cloth	0.5 M H <sub>2</sub> SO <sub>4</sub>	59		58	51
Ni-Co-P HNBS	Ni foam	1.0 M KOH	107		46	52
Multishelled Ni <sub>2</sub> P	Glassy carbon	1.0 M KOH	98		86.4	57
Ni(OH) <sub>2</sub> -Fe <sub>2</sub> P	Ti mesh	1.0 M KOH	76		105	62
CeO <sub>2</sub> -Cu <sub>3</sub> P	Ni foam	1.0 M KOH		148	132	64
PANI/CoP HNWS	Carbon fibers	0.5 M H <sub>2</sub> SO <sub>4</sub>	57	82	34.5	66
Fe-CoP	Ti foil	1.0 M KOH	78		75	67
P-Fe <sub>2</sub> N/rGO	Glassy carbon	0.5 M H <sub>2</sub> SO <sub>4</sub>	64.8		48.7	68
P-Ag@NC	Glassy carbon	0.5 M H <sub>2</sub> SO <sub>4</sub>	78		107	69
np-CoP <sub>3</sub>	Ti mesh	1.0 M KOH	76		45	70
CoP/CeO <sub>2</sub>	Ti mesh	1.0 M KOH	43		45	71
MoP/CNTs	Glassy carbon	0.5 M H <sub>2</sub> SO <sub>4</sub>	41		51.6	72
HI-CoP/CNT	Glassy carbon	0.5 M H <sub>2</sub> SO <sub>4</sub>	73		54.6	73
P-Mo <sub>2</sub> C@C	Glassy carbon	0.5 M H <sub>2</sub> SO <sub>4</sub>	89		42	74
CoP <sub>2</sub>	Carbon cloth	0.5 M H <sub>2</sub> SO <sub>4</sub>	56	86	67	75
porous Ni <sub>2</sub> P	Glassy carbon	1.0 M KOH	168		63	76

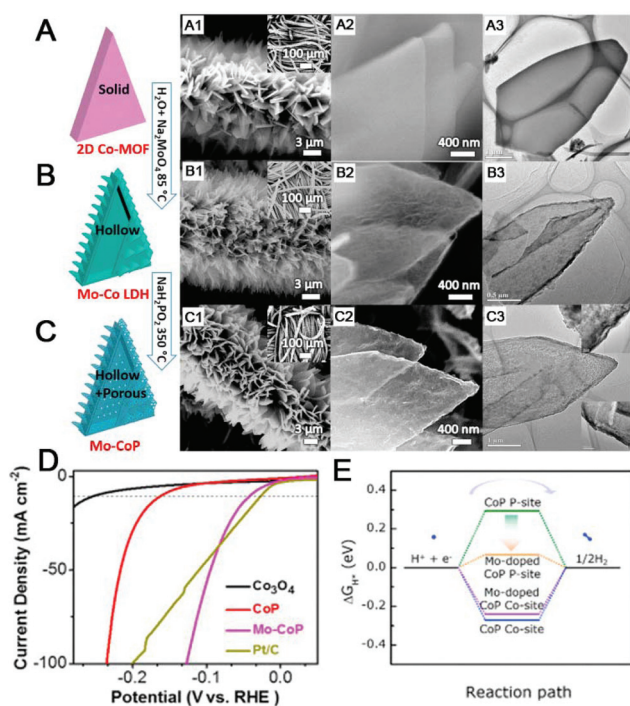


**Fig. 2** Schematic fabrication process of the MOF-derived route and the resulting microstructures for hollow Mo-CoP nanoarrays. (A) Co-MOF arrays. (B) Mo-Co LDH. (C) Mo-CoP nanoarrays. (D) Polarization curves of Pt/C, Co<sub>3</sub>O<sub>4</sub>, CoP and Mo-CoP in 1.0 M KOH. (E) HER free energy diagrams of the P- and Co-sites on pristine and Mo-doped CoP (111) surfaces. Reproduced with permission from ref. 40, Copyright 2018 Elsevier Ltd.

all pH values.<sup>42</sup> The X-ray powder diffraction (XRD) analysis indicated the successful doping of Mn. The as-prepared Mn-Ni<sub>2</sub>P possessed lower thermo-neutral hydrogen adsorption free energy, thus enhancing the HER activity of Ni<sub>2</sub>P. Tuning the electronic structure is another reason for enhanced catalytic activity by metallic element doping. Recently, our group found that the HER activity of Ni<sub>2</sub>P can be enhanced by Al doping. The changes in the electronic structure were confirmed by X-ray photoelectron spectroscopy (XPS) analysis, and they promoted the enhancement of catalytic performance.<sup>39</sup>

## 2.2. Non-metallic element doping

Non-metallic element doping is also accessible to enhance the HER activity of TMPs. Zhou *et al.* prepared a N-doped CoP catalyst grown on carbon cloth (CC).<sup>45</sup> A hydrothermal route was first employed to coat the Co(OH)F precursor onto the carbon cloth and then the precursor was phosphated in two gases of pure Ar or Ar/NH<sub>3</sub>, yielding CoP/CC or N-CoP/CC, respectively (Fig. 3A). As revealed by the SEM image (Fig. 3B) and XRD patterns (Fig. 3C), the N-CoP catalyst was obtained. To afford a current density of 10 mA cm<sup>-2</sup> in 0.5 M H<sub>2</sub>SO<sub>4</sub>, N-CoP/CC needed an overpotential of 42 mV, which was lower than that of CoP/CC (85 mV, Fig. 3D). The Tafel slope of N-CoP/CC (41.2 mV dec<sup>-1</sup>) was also lower than that of CoP/CC (50.5 mV dec<sup>-1</sup>), indicating the enhanced intrinsic catalytic activity (Fig. 3E). The authors claimed that the N-doping could modulate the electronic structure of orthorhombic CoP and tune the H adsorption on the CoP surface (Fig. 3F). The adsorption

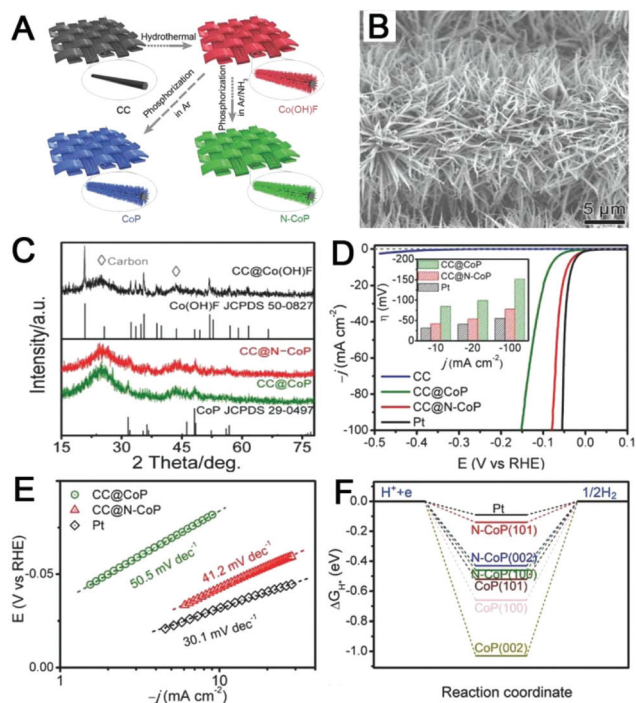


**Fig. 3** (A) Schematic fabrication process of CoP and N-CoP on carbon cloth. (B) SEM image of N-CoP/CC. (C) XRD patterns of the as-prepared samples. (D) Polarization curves of Pt/C, CC, CoP and N-CoP in 0.5 M H<sub>2</sub>SO<sub>4</sub>. (E) Tafel plots of Pt/C, CoP and N-CoP in 0.5 M H<sub>2</sub>SO<sub>4</sub>. (F) Free energy diagram for hydrogen (H<sup>\*</sup>) adsorption at the Co–Co bridge site on several low-index planes of CoP with and without N doping. Reproduced with permission from ref. 45, Copyright 2018 Wiley-VCH.

energy was tuned close to be thermo-neutral and significantly reduced the overpotential of the HER. Besides this, other non-metallic elements (such as S, P and Se) also proved as efficient dopants for enhancing HER catalytic activity.<sup>46–48</sup> The reasons for the high catalytic activity of the doped materials are elucidated by means of experimental verification and DFT calculations, and tuning the electronic structure and adsorption energy are suggested reasons.

### 2.3. Hybridization with other compositions

Hybrid materials are prepared by hybridizing two different compositions by the straightforward strategies (such as the hydrothermal method, chemical vapor deposition method and electrochemical deposition method). Generally, the hybrid catalyst showed more efficient activity due to the strong synergistic effect between the different compositions and the enhanced mass transportation ability.<sup>49</sup> The Li group and co-workers developed a Ni<sub>2</sub>P–CoP hybrid nanosheet array through an electrochemical deposition route as the efficient cathode for hydrogen evolution.<sup>49</sup> The resulting Ni<sub>2</sub>P–CoP hybrid catalyst presented enhanced HER activity compared to Ni<sub>2</sub>P and CoP. The authors confirmed the presence of strong electron interactions and synergistic effects between Ni<sub>2</sub>P and CoP by XPS analysis. These two points are important for enhancing catalytic performance. Yu *et al.* prepared a FeP/Ni<sub>2</sub>P hybrid

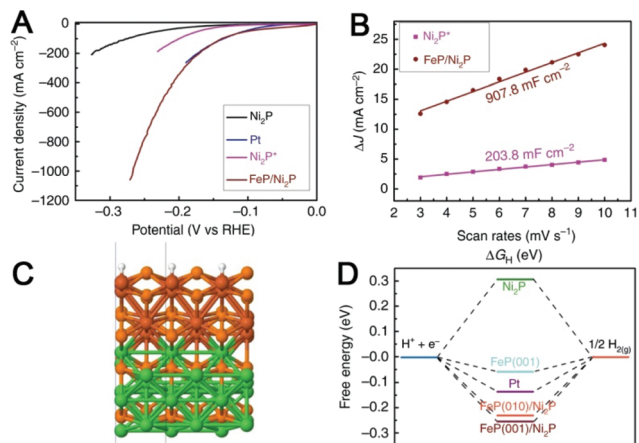


**Fig. 4** (A) Polarization curves of Pt/C, Ni<sub>2</sub>P and FeP/Ni<sub>2</sub>P in 1.0 M KOH. (B) Double-layer capacitance measurements for determining electrochemically active surface areas of Ni<sub>2</sub>P and FeP/Ni<sub>2</sub>P electrodes. (C) FeP (001) on Ni<sub>2</sub>P (100), side view. (D) Free energy diagram of  $\Delta G_{\text{H}}$ , the hydrogen adsorption free energy at pH = 14 on the FeP/Ni<sub>2</sub>P catalyst in comparison with Ni<sub>2</sub>P and benchmark Pt catalysts. Reproduced with permission from ref. 50, Copyright 2018 Nature Publishing Group.

catalyst by the chemical vapor deposition method.<sup>50</sup> The elemental mapping showed that Fe, Ni and P elements were evenly distributed throughout the whole catalyst surface. The FeP/Ni<sub>2</sub>P hybrid catalyst possessed Pt-like hydrogen evolution catalytic performance in 1.0 M KOH (Fig. 4A). The double layer capacitance ( $C_{\text{dl}}$ ) of FeP/Ni<sub>2</sub>P (907.8 mF cm<sup>-2</sup>) was bigger than that of pure Ni<sub>2</sub>P (203.8 mF cm<sup>-2</sup>, Fig. 4B), indicating a more rough surface of FeP/Ni<sub>2</sub>P. Furthermore, the authors hypothesized that the as-synthesized FeP nanoparticles along with Ni<sub>2</sub>P preferentially exposed the most active facets as those of the bulk FeP (001) crystals, and DFT calculations indicated that the FeP (001) crystals contributed to the high activity (Fig. 4C and D). A similar structure of Cu<sub>3</sub>P–CoP directly grown on CC *via* low-temperature phosphidation was reported by our group, and the Cu<sub>3</sub>P–CoP hybrid catalyst also showed enhanced HER activity in 0.5 M H<sub>2</sub>SO<sub>4</sub> due to the synergistic effects between Cu<sub>3</sub>P and CoP.<sup>51</sup> So it is attractive to explore other doping elements or compositions for higher HER activity and further explain the reasons for enhanced catalytic activity.

## 3. Structure engineering for enhancing HER performance

In addition to the element doping mentioned above, structure engineering is also a considerable strategy to enhance the HER performance of catalysts. Here, we take a look at three aspects: hollow structures, nanoarray structures and heterostructures.

### 3.1. Hollow structures

The fabrication of hollow TMP catalysts is also an efficient strategy to improve the intrinsic catalytic activity. Hollow structures bring many benefits to catalysts, such as the large

exposed surface and abundant mass diffusion pathways.<sup>52–56</sup> Recently, the Lou group and co-workers designed Ag-incorporated Ni–Co–P hollow nanobricks (HNBs) by a template-assisted strategy.<sup>52</sup> The hollow structure can be viewed from SEM and TEM images (Fig. 5A–H). The as-prepared Ni–Co–P HNBS exhibited significantly enhanced HER catalytic performance in comparison with the Ni–Co–P nanosheets in 1.0 M KOH (Fig. 5I). The Tafel slope of Ni–Co–P HNBS ( $46 \text{ mV dec}^{-1}$ ) was also lower than that of Ni–Co–P nanosheets ( $53 \text{ mV dec}^{-1}$ ), indicating the enhanced intrinsic catalytic activity (Fig. 3H). The hollow structure in nanobricks facilitated free infiltration of the electrolyte and the mass transport, therefore improving the catalytic performance. Sun *et al.* reported hollow Ni<sub>2</sub>P microspheres as an active catalyst for hydrogen evolution.<sup>57</sup> The as-prepared catalyst showed enhanced catalytic performance, and the large exposed surface offered more active sites, thus facilitating the reaction. All these examples indicate that the electrochemical active surface area can be increased by constructing a hollow structure, thus further improving the HER performance.<sup>52,53,55,58</sup>

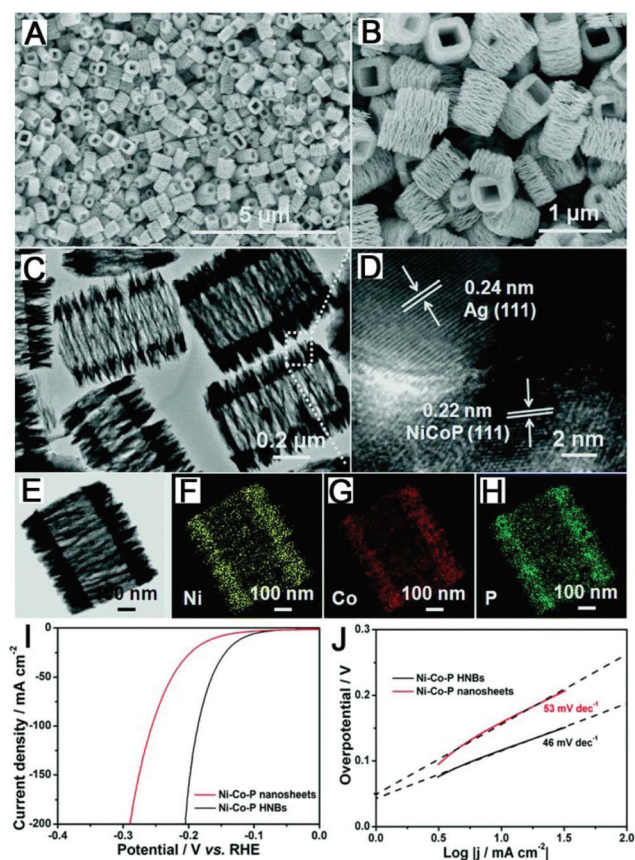


Fig. 5 (A and B) FESEM, (C) TEM, (D) HRTEM, and (E) STEM images of the hierarchical Ni–Co–P HNBS fabricated by a template-assisted strategy. Elemental mapping images of (F) Ni, (G) Co, and (H) P for the single Ni–Co–P HNB in (E). (I) Polarization curves and (J) Tafel plots of the hierarchical Ni–Co–P HNBS and Ni–Co–P nanosheets for HER in 1.0 M KOH. Reproduced with permission from ref. 52, Copyright 2018 Royal Society of Chemistry.

### 3.2. Nanoarray structures

In recent years, self-supported nanoarrays are becoming more and more popular in electrocatalysts research studies.<sup>11,30,31,45</sup> Nanoarrays usually include nanowires, nanosheets, nanorods, *etc.* These nanoarrays can always exhibit much better catalytic performance compared to planar ones. The large and rough surface area increases the contact area between the catalyst and the electrolyte, and thus effectively enhances the catalytic performance. Tian *et al.* reported the topotactic fabrication of self-supported Cu<sub>3</sub>P nanowire arrays on Cu foam (CF).<sup>30</sup> Fig. 6A presents the SEM image of Cu(OH)<sub>2</sub>/CF, the nanowire nature was maintained after phosphating (Fig. 6B and C). Cu<sub>3</sub>P nanowire arrays showed enhanced HER activity compared to Cu<sub>3</sub>P microparticles in 0.5 M H<sub>2</sub>SO<sub>4</sub> due to the large *C*<sub>dl</sub> and surface area (Fig. 6D). A FeP nanowire array was synthesized from its hydroxide precursor through low-temperature phosphidation.<sup>31</sup> Fig. 6E–G shows SEM images of the FeP nanowire array. The obtained catalyst possessed superior HER performance due to the large contact area between the catalyst and the electrolyte (Fig. 6H). Generally, the use of self-supported nanoarray catalysts can greatly increase the current density at the same overpotential.

### 3.3. Heterostructures

The construction of heterostructures has been demonstrated as an efficient method to enhance the HER performance, because the accompanying interface effect makes the (hydroxide) oxide behave as water dissociation promoters in metal catalysts.<sup>59–63</sup> Wang *et al.* developed a CeO<sub>2</sub>–Cu<sub>3</sub>P nanosheet array grown on Ni foam with enhanced catalytic activity for alkaline hydrogen evolution.<sup>64</sup> DFT calculations revealed that the CeO<sub>2</sub>–Cu<sub>3</sub>P interface promoted the water dissociation and resulted in a more thermo-neutral hydrogen adsorption free

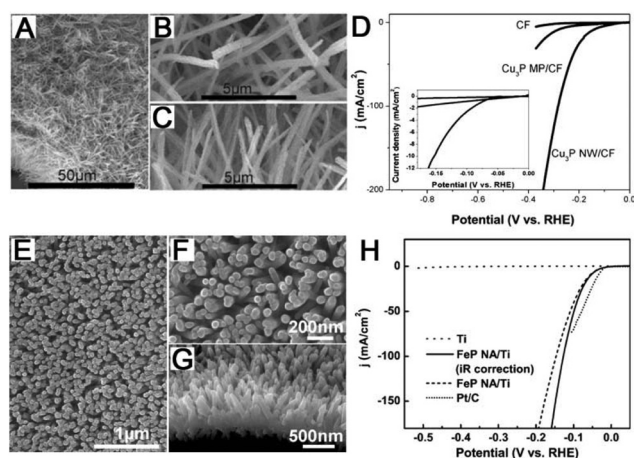


Fig. 6 (A) SEM image of Cu(OH)<sub>2</sub>/CF. (B and C) SEM images of Cu<sub>3</sub>P/CF. (D) Polarization curves of CF, Cu<sub>3</sub>P nanowires/CF and Cu<sub>3</sub>P microparticles/CF in 0.5 M H<sub>2</sub>SO<sub>4</sub> at a scan rate of  $2 \text{ mV s}^{-1}$ . (E–G) SEM images of FeP/Ti. (H) Polarization curves of Ti and FeP nanowires/Ti in 0.5 M H<sub>2</sub>SO<sub>4</sub> at a scan rate of  $2 \text{ mV s}^{-1}$ . Reproduced with permission from ref. 30 and 31, Copyright 2014 Wiley-VCH.

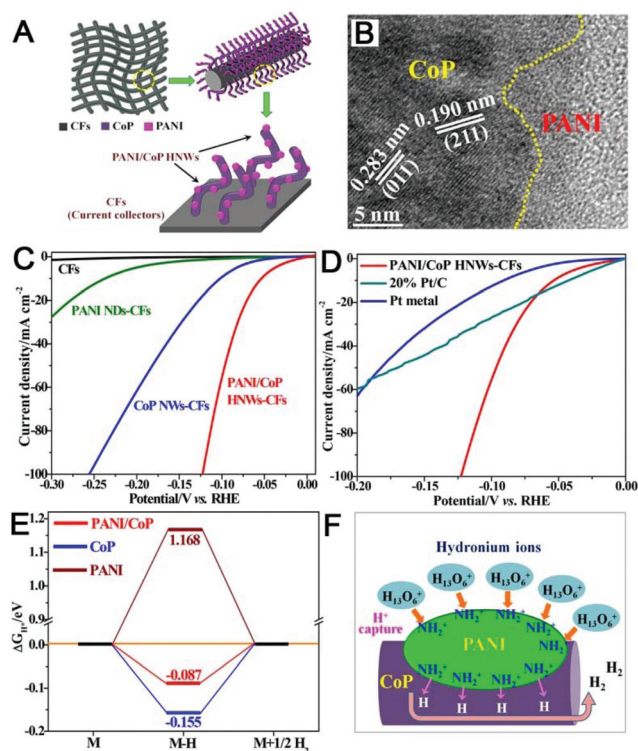


Fig. 7 (A) Schematic illustration of the structure of PANI/CoP HNWs-CFs. (B) HRTEM image of PANI NDs/CoP HNWs. (C, D) Polarization curves of PANI/CoP HNWs-CFs, PANI NDs-CFs, CoP NWs-CFs, CFs, Pt metal (loading:  $4.5 \text{ mg cm}^{-2}$ ) and 20 wt% Pt/C (loading:  $0.012 \text{ mg cm}^{-2}$ ) in  $0.5 \text{ M H}_2\text{SO}_4$ . (E) Free energy profile of H adsorption on the different catalysts. (F) Scheme of HER improvement by capturing the  $\text{H}^+$  in the hydronium ions to form the protonated amine groups on PANI/CoP HNWs. Reproduced with permission from ref. 66, Copyright 2018 American Chemical Society.

energy, thus, the catalytic activity was improved by interface engineering. Under acidic conditions, the positive charge density of  $\text{H}^+$  can be reduced by the coordinated water molecules in hydronium ions,<sup>65</sup> resulting in a low overpotential of the HER on catalysts. The Li group reported polyaniline (PANI) nanodot-decorated CoP hybrid nanowires grown on carbon fibers (PANI/CoP HNWs-CFs, as illustrated in Fig. 7A and B, which presented Pt-like HER activity in  $0.5 \text{ M H}_2\text{SO}_4$  (Fig. 7C and D).<sup>66</sup> The amine groups in PANI can easily capture the  $\text{H}^+$  in the hydronium ions and thus increase the concentration of  $\text{H}^+$  on the surface of the catalyst. As a result, the PANI/CoP hybrids showed impressive HER activity. The DFT calculations suggested that PANI/CoP hybrids could optimize H adsorption to improve their performance (Fig. 7E and F).

## 4. Conclusions and perspectives

In conclusion, this mini review briefly summarizes the most recent and instructive developments in the design of TMP-based catalysts with enhanced HER activity. These strategies are highlighted from two aspects, the composition engineering

and the structure engineering. From recent studies, it has been clearly confirmed that the above-mentioned strategies are useful for optimizing the intrinsic activity of catalysts. In the section on composition engineering, we summarized the catalytic performance changes caused by element doping and hybridization with other compositions. Regarding structure engineering, we point out that the excellent catalytic performance benefits from the optimized H adsorption, the large exposed surface and abundant mass diffusion pathways. The strategies mentioned above are not only useful for enhancing the catalytic activity of TMP-based catalysts, but meaningful for designing other inexpensive and high-performance catalysts.

In addition, TMPs have been proven to be effective catalysts for the HER, but the real mechanism of the HER still deserves much exploration. The current work mainly focuses on characterizing the morphology and electrochemical performance and thus the mechanism is not sufficiently understood. More attention should be paid to exploring the mechanism of TMPs in the catalytic reaction process. On one hand, the combination of works with modern advanced characterization techniques can guarantee the accuracy of the analysis. On the other hand, taking full advantage of DFT calculations can help us gain insight into the catalytic mechanism. Furthermore, TMP-based catalysts also arouse research interest towards many other fields of energy conversion and storage, such as batteries. In the immediate future, we anticipate that TMP-based catalysts can be used in actual industrial production to solve energy problems.

## Conflicts of interest

There are no conflicts to declare.

## Acknowledgements

This work was supported by the National Natural Science Foundation of China (21775089), Outstanding Youth Foundation of Shandong Province (ZR2017JL010), and the Natural Science Foundation Projects of Shandong Province (ZR2017QB008).

## References

- 1 J. Chow, R. J. Kopp and P. R. Portney, *Science*, 2003, **302**, 1528–1531.
- 2 M. S. Faber and S. Jin, *Energy Environ. Sci.*, 2014, **7**, 3519–3542.
- 3 Y. Jiao, Y. Zheng, M. Jaroniec and S. Z. Qiao, *Chem. Soc. Rev.*, 2015, **44**, 2060–2086.
- 4 Z. Wang, X. Ren, Y. Luo, L. Wang, G. Cui, F. Xie, H. Wang, Y. Xie and X. Sun, *Nanoscale*, 2018, **10**, 12302–12307.
- 5 Y. Zheng, Y. Jiao and S. Z. Qiao, *Adv. Mater.*, 2015, **27**, 5372–5378.

- 6 Z. Wang, Z. Liu, G. Du, A. M. Asiri, L. Wang, X. Li, H. Wang, X. Sun, L. Chen and Q. Zhang, *Chem. Commun.*, 2018, **54**, 810–813.
- 7 Z. Xi, A. Mendoza-Garcia, H. Zhu, M. Chi, D. Su, D. P. Erdosy, J. Li and S. Sun, *Green Energy Environ.*, 2017, **2**, 119–123.
- 8 Z. Wang, X. Ren, X. Shi, A. M. Asiri, L. Wang, X. Li, X. Sun, Q. Zhang and H. Wang, *J. Mater. Chem. A*, 2018, **6**, 3864–3868.
- 9 L. Wu, Q. Li, C. H. Wu, H. Zhu, A. Mendoza-Garcia, B. Shen, J. Guo and S. Sun, *J. Am. Chem. Soc.*, 2015, **137**, 7071–7074.
- 10 G. Zhang, Q. Ji, Z. Wu, G. Wang, H. Liu, J. Qu and J. Li, *Adv. Funct. Mater.*, 2018, **28**, 1706462.
- 11 J. Tian, Q. Liu, A. M. Asiri and X. Sun, *J. Am. Chem. Soc.*, 2014, **136**, 7587–7590.
- 12 Q. Li, L. Wu, G. Wu, D. Su, H. Lv, S. Zhang, W. Zhu, A. Casimri, H. Zhu, A. Mendoza-Garcia and S. Sun, *Nano Lett.*, 2015, **15**, 2468–2473.
- 13 C. Wu, D. Liu, H. Li and J. Li, *Small*, 2018, **14**, 1704227.
- 14 X. Zou and Y. Zhang, *Chem. Soc. Rev.*, 2015, **44**, 5148–5180.
- 15 A. J. Bard and L. R. Faulkner, *Electrochemical Methods: Fundamentals and Applications*, Wiley, New York, 2001.
- 16 J. O. Bockris, A. K. N. Reddy and M. E. Gamboa-Aldeco, *Modern Electrochemistry*, Plenum Press, New York, 1998.
- 17 M. Zeng and Y. Li, *J. Mater. Chem. A*, 2015, **3**, 14942–14962.
- 18 Y. Yan, B. Y. Xia, B. Zhao and X. Wang, *J. Mater. Chem. A*, 2016, **4**, 17587–17603.
- 19 E. J. Popczun, C. G. Read, C. W. Roske, N. S. Lewis and R. E. Schaak, *Angew. Chem., Int. Ed.*, 2014, **53**, 5427–5430.
- 20 H. Yang, Y. Zhang, F. Hu and Q. Wang, *Nano Lett.*, 2015, **15**, 7616–7620.
- 21 M. Cabán-Acevedo, M. L. Stone, J. R. Schmidt, J. G. Thomas, Q. Ding, H. C. Chang, M. L. Tsai, J. H. He and S. Jin, *Nat. Mater.*, 2015, **14**, 1245–1251.
- 22 F. H. Saadi, A. I. Carim, W. S. Drisdell, S. Gul, J. H. Baricuatro, J. Yano, M. P. Soriaga and N. S. Lewis, *J. Am. Chem. Soc.*, 2017, **139**, 12927–12930.
- 23 T. R. Hellstern, J. D. Benck, J. Kibsgaard, C. Hahn and T. F. Jaramillo, *Adv. Energy Mater.*, 2016, **6**, 1501758.
- 24 E. J. Popczun, J. R. McKone, C. G. Read, A. J. Biacchi, A. M. Wiltrout, N. S. Lewis and R. E. Schaak, *J. Am. Chem. Soc.*, 2013, **135**, 9267–9270.
- 25 Z. Pu, Q. Liu, C. Tang, A. M. Asiri and X. Sun, *Nanoscale*, 2014, **6**, 11031–11034.
- 26 L. Feng, H. Vruble, M. Bensimon and X. Hu, *Phys. Chem. Chem. Phys.*, 2014, **16**, 5917–5921.
- 27 J. Kibsgaard and T. F. Jaramillo, *Angew. Chem., Int. Ed.*, 2014, **53**, 14433–14437.
- 28 P. Xiao, M. A. Sk, L. Thia, X. M. Ge, R. J. Lim, J. Y. Wang, K. H. Lim and X. Wang, *Energy Environ. Sci.*, 2014, **7**, 2624–2629.
- 29 J. M. McEnaney, J. C. Crompton, J. F. Callejas, E. J. Popczun, A. J. Biacchi, N. S. Lewis and R. E. Schaak, *Chem. Mater.*, 2014, **26**, 4826–4831.
- 30 J. Tian, Q. Liu, N. Cheng, A. M. Asiri and X. Sun, *Angew. Chem., Int. Ed.*, 2014, **53**, 9577–9581.
- 31 P. Jiang, Q. Liu, Y. Liang, J. Tian, A. M. Asiri and X. Sun, *Angew. Chem., Int. Ed.*, 2014, **53**, 12855–12859.
- 32 J. F. Callejas, J. M. McEnaney, C. G. Read, J. C. Crompton, A. J. Biacchi, E. J. Popczun, T. R. Gordon, N. S. Lewis and R. E. Schaak, *ACS Nano*, 2014, **8**, 11101–11107.
- 33 A. B. Laursen, K. R. Patraju, M. J. Whitaker, M. Retuerto, T. Sarkar, N. Yao, K. V. Ramanujachary, M. Greenblatt and G. C. Dismukes, *Energy Environ. Sci.*, 2015, **8**, 1027–1034.
- 34 P. Liu and J. A. Rodriguez, *J. Am. Chem. Soc.*, 2005, **127**, 14871–14878.
- 35 Y. Xu, R. Wu, J. Zhang, Y. Shi and B. Zhang, *Chem. Commun.*, 2013, **49**, 6656–6658.
- 36 Y. Liang, Q. Liu, A. M. Asiri, X. Sun and Y. Luo, *ACS Catal.*, 2014, **4**, 4065–4069.
- 37 Z. Pu, Q. Liu, A. M. Asiri and X. Sun, *ACS Appl. Mater. Interfaces*, 2014, **6**, 21874–21879.
- 38 Y. Zheng, Y. Jiao, M. Jaroniec and S. Qiao, *Angew. Chem., Int. Ed.*, 2015, **54**, 52–65.
- 39 H. Du, L. Xia, S. Zhu, F. Qu and F. Qu, *Chem. Commun.*, 2018, **54**, 2894–2897.
- 40 C. Guan, W. Xiao, H. Wu, X. Liu, W. Zang, H. Zhang, J. Ding, Y. Feng, S. J. Pennycook and J. Wang, *Nano Energy*, 2018, **48**, 73–80.
- 41 H. Du, R. Kong, F. Qu and L. Lu, *Chem. Commun.*, 2018, **54**, 10100–10103.
- 42 X. Wang, H. Zhou, D. Zhang, M. Pi, J. Feng and S. Chen, *J. Power Sources*, 2018, **387**, 1–8.
- 43 T. Liu, D. Liu, F. Qu, D. Wang, L. Zhang, R. Ge, S. Hao, Y. Ma, G. Du, A. M. Asiri, L. Chen and X. Sun, *Adv. Energy Mater.*, 2017, **7**, 1700020.
- 44 D. Wang, M. Gong, H. Chou, C. Pan, H. Chen, Y. Wu, M. Lin, M. Guan, J. Yang, C. Chen, Y. Wang, B. Hwang, C. Chen and H. Dai, *J. Am. Chem. Soc.*, 2015, **137**, 1587–1592.
- 45 Q. Zhou, Z. Shen, C. Zhu, J. Li, Z. Ding, P. Wang, F. Pan, Z. Zhang, H. Ma, S. Wang and H. Zhang, *Adv. Mater.*, 2018, **30**, 1800140.
- 46 X. Ren, Q. Ma, H. Fan, L. Pang, Y. Zhang, Y. Yao, X. Ren and S. Liu, *Chem. Commun.*, 2015, **51**, 15997–16000.
- 47 J. Kibsgaard and T. F. Jaramillo, *Angew. Chem., Int. Ed.*, 2014, **53**, 14433–14437.
- 48 Z. Wang, H. Liu, R. Ge, X. Ren, J. Ren, D. Yang, L. Zhang and X. Sun, *ACS Catal.*, 2018, **8**, 2236–2241.
- 49 A. L. Wang, J. Lin, H. Xu, Y. X. Tong and G. R. Li, *J. Mater. Chem. A*, 2016, **4**, 16992–16999.
- 50 F. Yu, H. Zhou, Y. Huang, J. Sun, F. Qin, J. Bao, W. A. Goddard III, S. Chen and Z. Ren, *Nat. Commun.*, 2018, **9**, 2551.
- 51 H. Du, X. Zhang, Q. Tan, R. Kong and F. Qu, *Chem. Commun.*, 2017, **53**, 12012–12015.
- 52 E. Hu, Y. Feng, J. Nai, D. Zhao, Y. Hu and X. Lou, *Energy Environ. Sci.*, 2018, **11**, 872–880.
- 53 Y. Shi and B. Zhang, *Dalton Trans.*, 2017, **46**, 16770–16773.
- 54 J. Xu, D. Xiong, I. Amorim and L. Liu, *ACS Appl. Nano Mater.*, 2018, **1**, 617–624.

- 55 Y. Yang, M. Luo, Y. Xing, S. Wang, W. Zhang, F. Lv, Y. Li, Y. Zhang, W. Wang and S. Guo, *Adv. Mater.*, 2018, **30**, 1706085.
- 56 T. Wu, M. Pi, X. Wang, W. Guo, D. Zhang and S. Chen, *Appl. Surf. Sci.*, 2018, **427**, 800–806.
- 57 H. Sun, X. Xu, Z. Yan, X. Chen, F. Cheng, P. S. Weiss and J. Chen, *Chem. Mater.*, 2017, **29**, 8539–8547.
- 58 Y. Li, J. Liu, C. Chen, X. Zhang and J. Chen, *ACS Appl. Mater. Interfaces*, 2017, **9**, 5982–5991.
- 59 M. K. Bates, Q. Jia, N. Ramaswamy, R. J. Allen and S. Mukerjee, *J. Phys. Chem. C*, 2015, **119**, 5467–5477.
- 60 H. Jin, J. Wang, D. Su, Z. Wei, Z. Pang and Y. Wang, *J. Am. Chem. Soc.*, 2015, **137**, 2688–2694.
- 61 J. Feng, H. Xu, Y. Dong, X. Lu, Y. Tong and G. Li, *Angew. Chem., Int. Ed.*, 2017, **56**, 2960–2964.
- 62 X. Zhang, S. Zhu, L. Xia, C. Si, F. Qu and F. Qu, *Chem. Commun.*, 2018, **54**, 1201–1204.
- 63 X. Guo, R. Kong, X. Zhang, H. Du and F. Qu, *ACS Catal.*, 2018, **8**, 651–655.
- 64 Z. Wang, H. Du, Z. Liu, H. Wang, A. M. Asiri and X. Sun, *Nanoscale*, 2018, **10**, 2213–2217.
- 65 E. S. Stoyanov, I. V. Stoyanova and C. A. Reed, *J. Am. Chem. Soc.*, 2010, **132**, 1484–1485.
- 66 J. X. Feng, S. Y. Tong, Y. X. Tong and G. R. Li, *J. Am. Chem. Soc.*, 2018, **140**, 5118–5126.
- 67 C. Tang, R. Zhang, W. Lu, L. He, X. Jiang, A. M. Asiri and X. Sun, *Adv. Mater.*, 2017, **29**, 1602441.
- 68 P. Yu, L. Wang, Y. Xie, C. Tian, F. Sun, J. Ma, M. Tong, W. Zhou, J. Li and H. Fu, *Small*, 2018, **14**, 1801717.
- 69 X. Ji, B. Liu, X. Ren, X. Shi, A. M. Asiri and X. Sun, *ACS Sustainable Chem. Eng.*, 2018, **6**, 4499–4503.
- 70 Y. Ji, L. Yang, X. Ren, G. Cui, X. Xiong and X. Sun, *ACS Sustainable Chem. Eng.*, 2018, **6**, 11186–11189.
- 71 R. Zhang, X. Ren, S. Hao, R. Ge, Z. Liu, A. M. Asiri, L. Chen, Q. Zhang and X. Sun, *J. Mater. Chem. A*, 2018, **6**, 1985–1990.
- 72 A. Adam, M. H. Suliman, H. Dafalla, A. R. Al-Arfaj, M. N. Siddiqui and M. Qamar, *ACS Sustainable Chem. Eng.*, 2018, **6**, 11414–11423.
- 73 A. Adam, M. H. Suliman, M. N. Siddiqui, Z. H. Yamani, B. Merzougui and M. Qamar, *ACS Appl. Mater. Interfaces*, 2018, **10**, 29407–29416.
- 74 Z. Shi, K. Nie, Z. Shao, B. Gao, H. Lin, H. Zhang, B. Liu, Y. Wang, Y. Zhang, X. Sun, X. Cao, P. Hu, Q. Gao and Y. Tang, *Energy Environ. Sci.*, 2017, **10**, 1262–1271.
- 75 Y. Zhou, Y. Yang, R. Wang, X. Wang, X. Zhang, L. Qiang, W. Wang, Q. Wang and Z. Hu, *J. Mater. Chem. A*, 2018, **6**, 19038–19046.
- 76 Q. Wang, Z. Liu, H. Zhao, H. Huang, H. Jiao and Y. Du, *J. Mater. Chem. A*, 2018, **6**, 18720–18727.